Proceedings of the 21st ICSMGE, Vienna, Austria, 14 – 19 June 2026. Pistrol, Adam & Schweiger (eds.)
Published by: ÖGG, Austrian Society for Geomechanics, Salzburg, Austria, ISBN 978-3-9503898-4-5
https://doi.org/10.53243/ICSMGE2026-794

Type B1 Predictions of Slope Performance during Rainfall Using Numerical Analysis

Rupsa Roy, Beena Ajmera
Department of Civil, Construction and Environmental Engineering, Iowa State University, Ames, USA,
rupsaroy@iastate.edu; bajmera@iastate.edu

Željko Arbanas, **Josip Peranić**
Faculty of Civil Engineering, University of Rijeka, Rijeka, Croatia
josip.peranic@gradri.uniri.hr; zeljko.arbanas@gradri.uniri.hr

ABSTRACT: In recent times, changes in rainfall patterns have led to an increase in the occurrence of high intensity rainfall events, triggering landslides, causing loss of life and property. This has necessitated the need for improved slope performance and early warning systems. While most studies have focused on post failure (Type C and C1) predictions, few studies have examined slope performance before or during the events, where the results remain unknown. This research aims to explore the relationship between prediction methods and the types of available data by focusing on predicting the performance of a Z shaped slope subjected to rainfall using numerical analysis. An experimental study was conducted on a coarse-grained soil Z-shaped slope, monitoring two key hydrological responses, the change in volumetric water content, which leads to slope saturation, and the time taken by slope to reach saturation. A Type B1 prediction method using a coupled pore pressure - stress analysis with a drained Mohr-Coulomb constitutive soil model was adopted in the GeoStudio suite software in order to predict slope performance. These predictions were then compared to experimental outcomes to evaluate the reliability of the numerical modeling approach. The results indicated finite element model (FEM) to effectively capture the volumetric water content response across all monitored slope segments, with close agreement observed at shallow depths (6 cm and 12 cm) and in the lower segment (toe) of the slope. However, the FEM overestimated the volumetric moisture content at depth (18 cm and 24 cm) in the upper and middle segments by 1.19 to 1.48 times, due to the assumption of uniform soil properties. FEM also successfully predicted time to submerge the toe with 5.1% margin of error, confirming the potential for simulating rainfall induced slope responses with limited initial input data.

KEYWORDS: Type B-1 prediction, rainfall induced slope failures, hydrological responses, finite element, numerical analysis, physical modeling.

1 INTRODUCTION

In recent years, the rise in the frequency and intensity of extreme rainfall events, often caused by atmospheric rivers and hurricane induced storms, have significantly increased the risk of rainfall induced landslides. Slope failures not only affect critical infrastructure but also pose severe threats to human life and property. Thus, accurate predictions of slope performance during such events have become a critical component of hazard mitigation and early warning systems.

Five predictive approaches in geotechnical engineering were proposed by Lambe (1973) which include types: A, B, B1, C, and C1. Predictions made prior to an event, based on known input data, are categorized as Type A. Type B and B1 correspond to predictions made before or during the occurrence on the event, based on limited input data. In contrast, Type C and C1 predictions are conducted after the event has occurred, with both the input data and actual outcomes known. Among these, Type C and C1 predictions (post-failure analysis) have been most commonly applied in slope stability studies, usually in the form of back analyses. These analyses are conducted after the event has occurred when the outcomes are already known. For example, Dai et al. (2023) performed a detailed post-failure analysis of the Ludoialm Landslide in Austria, highlighting the critical impact of hydrogeological heterogeneity in triggering a landslide. Genevois et al. (2022) investigated slope failures in the Dolomites region of Italy. Type C analyses showed that failures at sites such as Fiames and Perarolo were, respectively, due to the incomplete implementation of protective measures or underestimates of the subsurface complexity. While useful to understand the failure mechanisms and to calibrate models, Types C and C1 predictions provide limited benefit in terms of real time hazard mitigation.

Type A predictions, which are made before any failure occurs and without knowledge of the eventual outcome, have proven valuable in risk management and early intervention. A prominent example is the James Bay Dikes project, where Type A prediction methods successfully forecasted slope instability before its occurrence (Lambe, 1973). Smith et al. (2016) demonstrated another innovative application of Type A prediction using acoustic emission (AE) monitoring in large-scale slope models. While effective, the sensitivity of method to soil properties and limitations under very slow slope movements were acknowledged.

Previous research has highlighted advancements in Type A and Types C or C1 prediction methodologies, but a critical gap remains in bridging pre-event simulations with real-time observational data, particularly for rainfall induced slope failures. Addressing this gap is essential to enhance the accuracy of early warning systems and improve the reliability of slope stability assessment under rainfall conditions. This research aims to address this gap by exploring the relationship between prediction methods and the types of available data through the application of a Type B1 prediction approach. This study integrates experimental observations and numerical simulations of a Z shaped slope inclined at 30^0 and subjected to controlled rainfall conditions. A coupled pore pressure–stress analysis in GeoStudio software with a drained Mohr-Coulomb model was adopted to examine the hydrological response of the slope. Limited laboratory data and model assumptions are used to evaluate the extent to which the finite element method (FEM) can capture the rainfall induced hydrological responses, highlighting the potential of Type B1 predictions in advancing real-time slope stability assessment.

2 METHODOLOGY

The study was carried out in two phases. In the first phase, an experimental Z shaped slope model was constructed and tested at the University of Rijeka, Croatia, to observe the hydrological response of the slope under controlled rainfall conditions. In the second phase, finite element numerical models replicating the

experimental slope geometry were developed at Iowa State University, USA, using the same boundary and loading conditions. When undertaking the second phase of this study, the results from the first phase were unknown to the associated authors. Rather, only limited laboratory data and assumptions were used in the numerical analyses. Hydrological responses obtained from both the experimental and numerical studies were compared to assess the predictive capability of the slope models.

2.1 *Experimental slope model*

Index properties of the soil used in the construction of the slope model, including particle size distribution, coefficient of permeability, and specific gravity were determined based on relevant ASTM standards. A summary of index properties of the soil used in the experimental slope model is presented in Table 1. Sieve analysis indicated all particles were between 0.075 mm and 4.75 mm in size, as indicated in Figure 1. In this study, the percentage of particles smaller than 4.75 mm and greater than 0.075 mm is defined as the sand fraction. The particle diameters corresponding to 60%, 30%, and 10% finer (d_{60}, d_{30}, and d_{10}) were observed to be 0.36 mm, 0.27 mm, and 0.10 mm, respectively. The coefficient of curvature (C_c) and coefficient of uniformity (C_u) were calculated to be 1.06 and 1.89, respectively. According to the Unified Soil Classification System (USCS), the soil was classified as a poorly graded sand (SP). The saturated hydraulic conductivity was determined using the constant head test and is provided in Table 1. Drained shear strength parameters were obtained through direct shear testing, following the procedures in ASTM D3080.

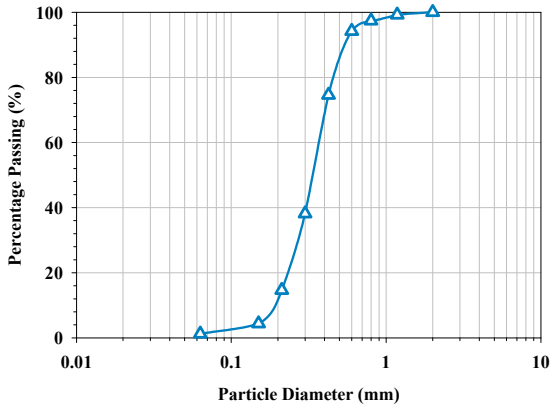

Figure 1. Particle size distribution curve for soil used in the experimental slope model.

Table 1. Index properties of soil used in slope.

Test	Standard	Soil
Particle Size Distribution	ASTM D6913	d_{60}= 0.36 mm d_{30}= 0.27 mm d_{10}= 0.10 mm
Constant Head Permeability	ASTM D2434	3.3 × 10^{-2} cm/sec
Direct Shear	ASTM D3080	Effective Cohesion = 0 kPa Effective Friction Angle= 35^0
Specific Gravity	ASTM D854	2.70
USCS Classification	ASTM D2487	SP

The Z shaped slope model inclined at 30°, as shown in Figure 2, was constructed within a Plexiglass container over a steel base plate. The slope was constructed from the bottom up and compacted in five uniform layers. Each layer was approximately 6 cm thick prepared with soil at an initial porosity of 44% and an initial gravimetric moisture content of 2.1%. After the slope was constructed, rainfall was applied using three nozzles positioned above the slope, applying a rainfall intensity of 79 mm/hr per square meter of the plan area. Drainage was not allowed in the model.

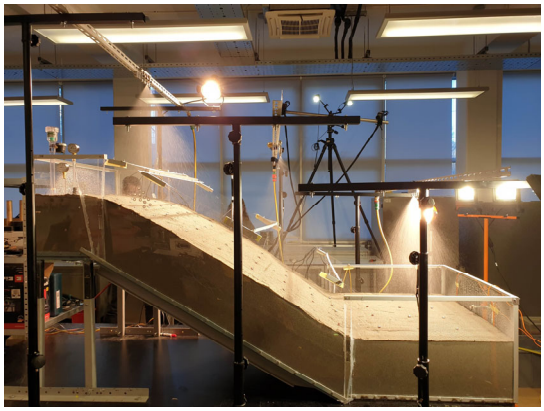

Figure 2. Z shaped experimental slope model inclined at 30°.

Two key hydrological responses, namely, the variation in volumetric water content across different regions with depth of the slope and the time required for the lower portion (toe) of the slope to reach saturation, were examined. The slope was instrumented with TEROS 10 and 12 (METER Group, Inc.) soil moisture sensors (theta probes), which were placed across the height of the slope relative to the impermeable steel base plate at the bottom of the model. The layout and locations of all sensors are shown in Figure 3. Water was allowed to accumulate at the base of the model, gradually raising the water level until the toe of the slope was submerged.

The slope was divided into three segments. The upper segment (H) is located at the midpoint of the horizontal bottom plate. Theta probes were installed at depths of 6 cm and 18 cm after compacting the second and fourth layers and are referred to as H-6 and H-18, respectively. The inclined segment (M) is located at one-third of the slope length along the inclined face. Theta probes were placed after the compaction of each layer at four measurement depths defined perpendicular to the base plate at M-6, M-12, M-18, and M-24. The lower segment (L) is located at the midpoint of the opposite end of the horizontal bottom plate. Four sensors were installed at depths of 6 cm, 12 cm, 18 cm, and 24 cm labeled as L-6, L-12, L-18, and L-24, respectively. All sensors were placed along the axis of symmetry of the slope model in the out-of-plane dimension to monitor temporal and spatial variations in volumetric water content during rainfall infiltration.

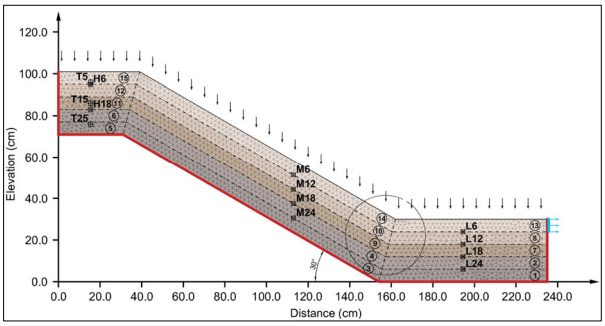

Figure 3. Location of theta probes in the experimental slope model.

2.2 *Numerical slope model*

The numerical model was developed using the GeoStudio Suite software (GEO-SLOPE International, 2015; Seequent Limited, 2024). During the development of the finite element model, the only known input parameters were the slope geometry, initial soil porosity, initial moisture content, particle size distribution, shear strength parameters, and the rainfall intensity. All other parameters required for the simulation were assumed based on literature or estimated using empirical methods.

The steps involved in numerical modeling are presented in Figure 4. First, the slope geometry was defined to have a 30° inclination and a Z shaped profile with a thickness of 30 cm. The locations of the theta probes at H, M, and L segments were specified within the model to match the experimental setup. Next, the initial pore-water pressure distribution in the slope model was obtained by performing a steady-state seepage analysis in SEEP/W. At this stage, the slope material was modeled as an unsaturated/saturated model. The soil water characteristic curve (SWCC) was defined using the grain-size-based estimation model in SEEP/W. The estimation approach is based on the modified Kovacs method, as proposed by Aubertin et al. (2003). For the coarse-grained soil in this study, the saturated volumetric water content was assumed to be 44% (equal to the porosity of the soil) with d_{10} and d_{60} (Table 1) used as inputs. The liquid limit was taken as zero. The maximum suction was assigned the default value of 1000 kPa. The resulting volumetric water content function is in Figure 5.

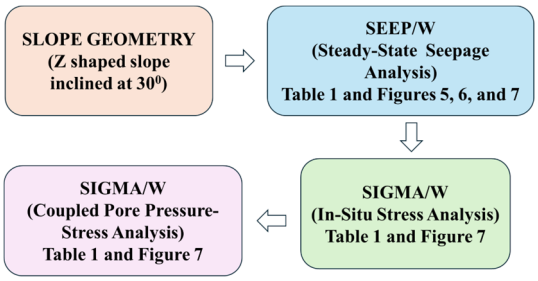

Figure 4. Steps adopted in the finite element numerical analysis.

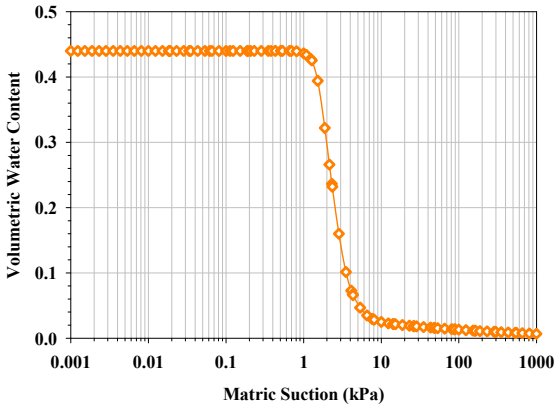

Figure 5. Soil water characteristic curve adopted in the numerical slope model.

The Van Genuchten model (1980) was adopted to define the hydraulic conductivity function in the numerical model, as shown in Figure 6. The soil-water characteristic curve (SWCC) was used to define the variation of hydraulic conductivity with matric suction. As the saturated hydraulic conductivity of the soil was not available when the finite element model was developed, it was estimated using the empirical relationship in Hazen (1982) given in Equation 1. In this equation, c is a constant ranging from 1.0 to 1.5. For this study, a conservative value of 1.0 was adopted. The resulting saturated permeability was 3.61×10^{-2} cm/sec. The residual volumetric water content was estimated from the SWCC (Figure 5) as 0.006. The initial boundary condition in the slope model was defined using the initial matric suction at an initial moisture content of 2.1%. Based on Figure 5, the initial suction was determined to be 5.5 kPa. This value was uniformly applied throughout the entire slope domain. A no flow boundary condition was assigned to the edges AB and EF, as well as the base of the slope (BCDE), as presented in Figure 7.

$$k_{sat}\left(\frac{cm}{sec}\right) = c.(d_{10})^2 \quad (1)$$

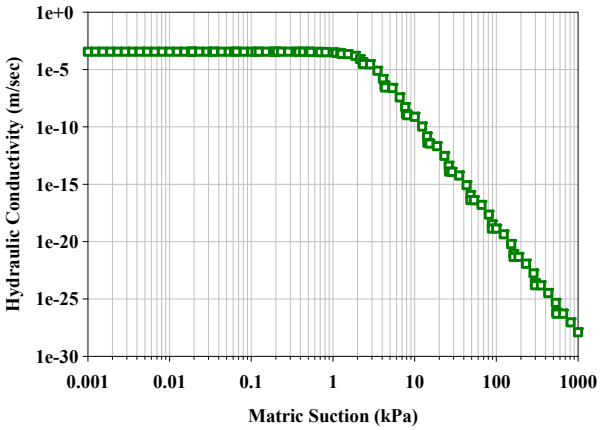

Figure 6. Hydraulic conductivity function adopted in the numerical slope model.

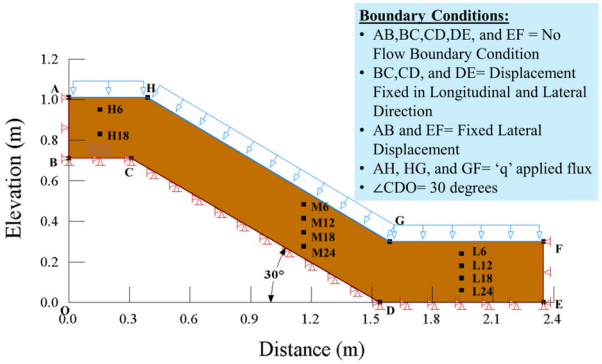

Figure 7. Slope geometry with boundary conditions in the numerical model.

An in-situ stress analysis in SIGMA/W provided the initial stress distribution in the model due to the self-weight of the slope. For this step, a drained Mohr-Coulomb constitutive soil model was adopted. The initial void ratio was estimated from the initial porosity to be 0.786. The initial unit weight of the soil was also computed based on the initial porosity and moisture content. The elastic modulus was assumed to be 50,000 kPa using Obrzud and Truty (2012). Poisson's ratio was assumed to be 0.25 (Essien et al. 2014 and Davidovici 1985). The friction angle was set at 35^0 (Table 1). Boundary conditions were applied by constraining lateral displacement along the two edges of the slope model while both the lateral and longitudinal displacements were restricted along the base of the model (Figure 7). A coupled pore pressure-stress analysis was then performed in SIGMA/W to capture the changes in the hydrological response of the slope when subjected to rainfall. Constant rainfall intensity of 79 mm/hr was applied as a unit hydraulic flux boundary flux (q) along the slope surface

(ABGF). The hydraulic and mechanical slope material models were retained from the SEEP/W and SIGMA/W analyses.

3 RESULTS AND DISCUSSION

3.1 *Volumetric Water Content Response at H*

Figure 8 presents the volumetric water content in the upper segment of the slope. The response was monitored over time at two depths, 6 cm and 18 cm, in both the experimental model (EXP) and the finite element model (FEM). At a depth of 6 cm, the experimental result indicated a rapid increase in volumetric water content, reaching approximately 0.21 within the first 20 to 30 minutes and then exhibited a constant value. In the FEM model, a similar initial trend in the volumetric water content was observed up to about 60 min. However, the volumetric water content in the FEM continued to steadily increase steadily reaching a value of 0.25 at 150 minutes, as shown in Figure 8a. The maximum value in the FEM model was approximately 1.19 times higher than that in the EXP model. This indicated the FEM results to be in close agreement with the EXP response at a shallow depth with the FEM slightly overestimating the water intake in the slope model.

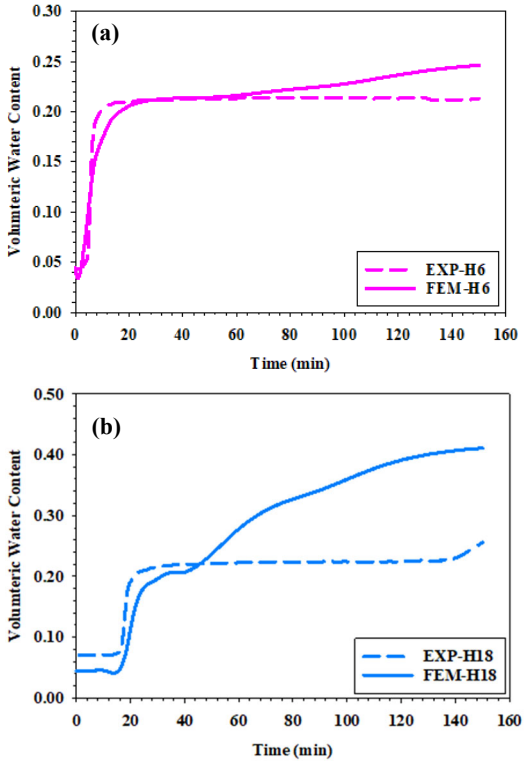

Figure 8. Volumetric water content in the H segment at depths of (a) 6 cm and (b) 18 cm.

The experimental data indicated a slower and stepped increase in volumetric water content at a depth of 18 cm depth, as shown in Figure 8b. The volumetric water content reached a constant value at 0.27 after approximately 75 minutes. The results from the FEM model were similar to the EXP results until about 50 min. However, the FEM model predicted a continuous increase in the volumetric water content with time. The values reaching up to 0.40 by the end of the simulation. However, the EXP results indicated that the volumetric water content remained constant over this time. Thus, the FEM overestimated the volumetric water content by 1.48 times. This might be attributed to modeling assumptions in which soil heterogeneity was not considered. Specifically, the FEM assumes that all the material properties are constant throughout the model. However, this is not truly the case in the experimental models, which will have some variability. Overall, the FEM model captured the volumetric water content response, but overestimated water retention more significantly as the depth increased.

3.2 *Volumetric Water Content Response at M*

Volumetric water content in the M slope segment was recorded at four depths (6 cm, 12 cm, 18, cm, and 24 cm). Figure 9 shows the volumetric water content response recorded in the experimental slope model and numerical simulations. At a depth of 6 cm, the experimental data showed a rapid increase in volumetric water content, which reached 0.26 within 30 minutes. It further increased to 0.33 in 90 minutes and then stabilized, as shown in Figure 9a. The FEM results followed a similar trend but predicted slightly higher values. Specifically, the volumetric water content from the FEM was recorded to be 0.44 by the end of the simulation, which is 1.29 times higher than that in the EXP model. At 12 cm depth, both the EXP and FEM models displayed a delayed response in reaching peak volumetric water content when compared to the responses at a depth of 6 cm. Experimental volumetric water content response, presented in Figure 9a, was observed to increase steeply before becoming constant at approximately 0.34. On the contrary, the FEM response peaked and stabilized at 0.44. Similar to results at depth of 6 cm, the FEM overestimated the moisture content by 1.29 times.

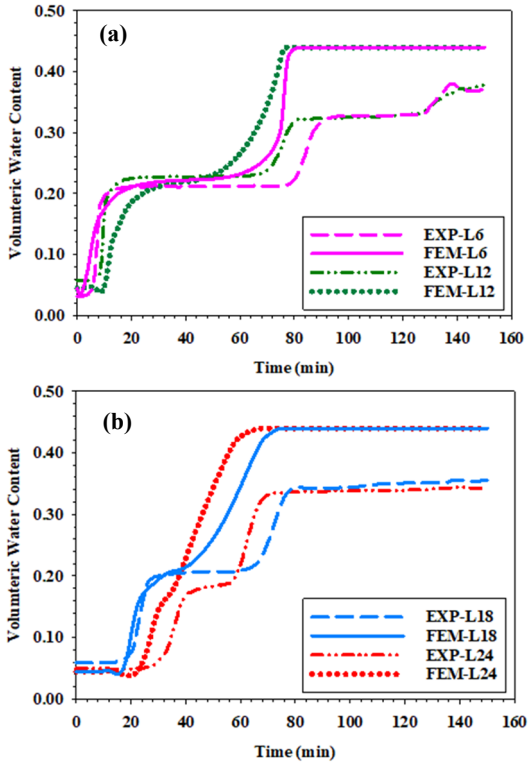

Figure 9. Volumetric water content in the M segment at depths of (a) 6 cm and 12 cm, and (b) 18 cm and 24 cm.

The EXP response indicated a rise in the moisture content at a depth of 18 cm stabilizing around 0.35, as shown in Figure 9b. In the contrary, the FEM prediction indicated a sharp rise in the volumetric water content, which reached 0.44 (1.25 times higher than that in the EXP model). The differences between experimental and numerical data became more pronounced as the depth increases. Specifically, at a depth of 24 cm, the EXP model (Figure 9b) indicated a gradual increase in volumetric moisture content that stabilized at 0.34. On the other hand, the FEM model predicted a significantly faster and higher increase

in volumetric water content stabilizing at 0.44. Overall, the FEM was able to capture the moisture variation trends across all depths but tends to overpredict the water content with more pronounced differences as the depth increases.

3.3 *Volumetric Water Content Response at L*

At a depth of 6 cm, the EXP measurements initially showed a steep increase in volumetric water content within the first 30 minutes, as shown in Figure 10a. It reached constant value of 0.25 before it started to increase again, stabilizing at 0.39 around 78 minutes. The FEM model closely followed the same trend reaching a volumetric water content of 0.44 in the same time. Thus, the volumetric water content was 1.12 times higher at the end of the FEM simulation in comparison to the EXP observations. At a depth of 12 cm, the difference in FEM and experimental response was observed to be more pronounced, as presented in Figure 10a. The EXP data indicated a rise in volumetric water content stabilizing at 0.34. In contrast, the FEM simulation showed a steeper rise in volumetric water content with value stabilizing at 0.44, which is 1.29 times higher.

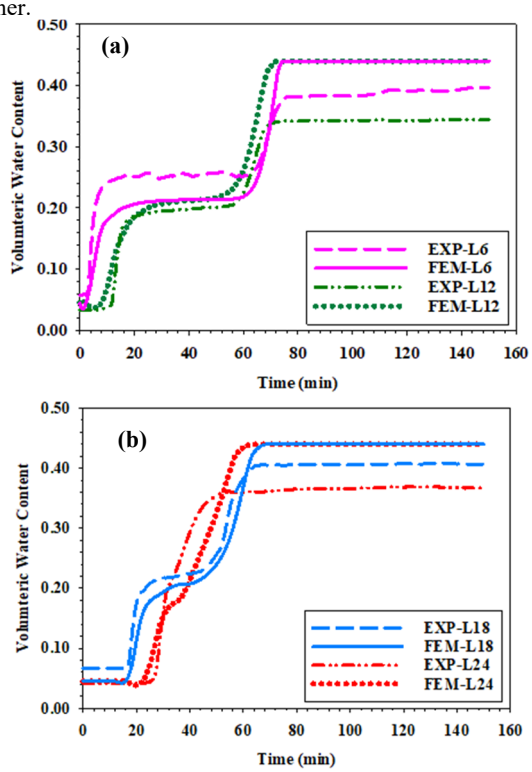

Figure 10. Volumetric water content in lower segment (L) in the experimental and numerical model at depths of (a) 6 cm and 12 cm, and (b) 18 cm and 24 cm.

Figure 10b shows the volumetric water content responses from the experimental and FEM models at depths of 18 cm and 24 cm. The EXP volumetric water content indicated a steep rise at a depth of 18 cm. It stabilized at approximately 0.40 in about 65 minutes. A similar response was observed in the FEM, which recorded the volumetric water content reaching 0.44 around the same time. At a depth of 24 cm, the EXP model showed a steady response with the final volumetric water content being around 0.36. The FEM results indicated a steeper response reaching about 0.44 in 65 minutes. At this depth, the FEM model overestimated the volumetric water content at the end of the simulation by 1.22 times the response recorded in the EXP model. Consistent with observations in H and M segments, the FEM model was observed to effectively captured the overall trends in moisture variation across all monitored depths in L segment, but overpredicts the volumetric water content. As noted before, this may be due to the limitations associated with the assumption of homogeneous soil conditions in the FEM. On the other hand, the limitations of theta probes in accurately measuring saturated volumetric water content is another factor that could affect the interpretation of the results in terms of moisture content.

3.4 *Toe Saturation Time*

As drainage was restricted by the impermeable steel base, the infiltrating rainwater entered the lower segment of the slope and began to build water pressure. After some time, the water level will rise upward and eventually submerging the toe of the slope. Based on experimental observations, the time required for the rainwater to reach and fully saturate the lower segment of the slope was approximately 79 minutes.

Figure 11 shows the development of pore pressure at the toe, where a change in pore pressure from negative to 0 kPa indicates the onset of saturation. The FEM predicted that the toe would become submerged at around 75 minutes, closely aligning with the experimental results. The error is approximately 5.1%. The corresponding pore pressure contours and phreatic surface in the FEM model are shown in Figure 12. The results in this figure confirm that the phreatic line, indicated by 0 kPa, reached the slope toe at this time.

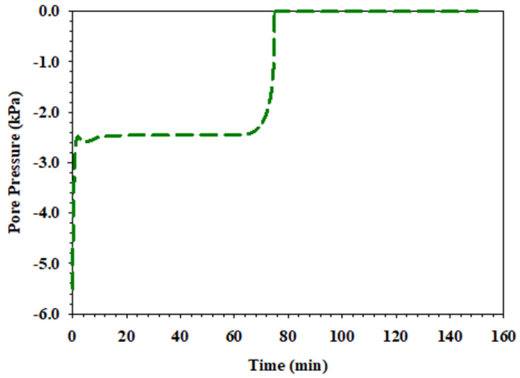

Figure 11. Pore pressure variation recorded at the toe of the slope in the FEM.

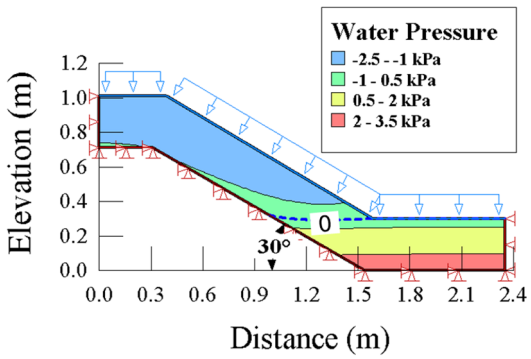

Figure 12. Pore pressure contour with phreatic line in the FEM model at 75 minutes.

4 CONCLUSIONS

For the Type B1 prediction undertaken in this study, the following conclusions are drawn by comparing the experimental and numerical results:

1. The finite element model was observed to successfully capture the volumetric water content trend across all monitored depths and slope segments (H, M, and L). The results were found to be in good agreement with the experimental data at shallow depths. However, the

FEM consistently overpredicted the cumulative volumetric water content in the slope models, with an increase in the amount of overprediction with an increase in depth.

2. In the upper and middle slope segments, the FEM model recorded a more gradual and higher accumulation of moisture when compared to the EXP observations. The overestimation in the volumetric water content ranged from 1.19 to 1.48 times, which became more pronounced as the depth increased. This indicated the sensitivity of FEM to soil stratification and heterogeneity, which could not be captured in the FEM model developed.
3. The volumetric water content variation in the lower slope segment indicated a good agreement between the FEM and EXP measurements. The FEM predictions were observed to be within 1.12 to 1.22 times of the EXP values, highlighting the ability of the model to replicate infiltration behavior more accurately in this zone.
4. The time required to the submerge the toe predicted in the FEM closely matched the EXP observations. This corresponded to 75 minutes in the FEM and 79 minutes in the EXP, which is associated with an error of 5.1%. This indicates the FEM to effectively model the cumulative pore pressure buildup and the advancement of phreatic surface.

A Type B1 prediction approach using coupled pore pressure–stress analysis with a drained Mohr-Coulomb model in GeoStudio was used to predict slope performance based on limited laboratory data available. The results validate the applicability of FEM in simulating rainfall induced hydrological responses, despite the assumptions adopted in the model. The results in the Type B1 predictions were based on very limited initial information. However, as more information is available at the onset of the numerical modelling, the expected results and errors from the FEM models are expected to reduce.

5 ACKNOWLEDGEMENTS

The authors would like to acknowledge the financial support provided to the first author by Deep Foundations Institute, NCMA Education and Research Foundation, and ADSC-The International Association of Foundation Drilling to support her doctoral studies. This work was supported by the International Consortium on Landslides under the project IPL-256, *Investigation of Landslide Initiation Caused by Rainfall Infiltration Using Small-Scale Physical and Numerical Modeling (ILIRIM)*, and by the University of Rijeka through the *uniri-iskusni-tehnic-23-240* project. This support is gratefully acknowledged. The authors also wish to express their sincere gratitude to the colleagues and students of the University of Rijeka, Faculty of Civil Engineering, who contributed to the experimental setup.

6 REFERENCES

ASTM International. (2023). ASTM D854-23: Standard Test Methods for Specific Gravity of Soil Solids by the Water Displacement Method.

ASTM International. (2021). ASTM D7928-17: Standard Test Method for Particle-Size Distribution (Gradation) of Fine-Grained Soils using the Sedimentation (Hydrometer) Analysis.

ASTM International. (2020). ASTM D2487-17: Standard Practice for Classification of Soils for Engineering Purposes (Unified Soil Classification System).

ASTM International. (2012). ASTM D3080: Standard Test Method for Direct Shear Test of Soils Under Consolidated Drained Conditions.

ASTM International. (2019). *ASTM D2434-68:* Standard Test Method for Permeability of Granular Soils (Constant Head).

Aubertin, M., Mbonimpa, M., Bussière, B., & Chapuis, R. P. (2003). A model to predict the water retention curve from basic geotechnical properties. *Canadian Geotechnical Journal*, 40(6), 1104–1122.

Davidovici, V. (1985) Génie parasismique. école Nationale des Ponts et Chaussees, Paris, 1105.

Dai, X., Schneider-Muntau, B., Krenn, J., Zangerl, C., and Fellin, W. (2023). Mechanisms for the formation of an exceptionally gently inclined basal shear zone of a landslide in glacial sediments—The Ludoialm case study. *Applied Sciences,* 13(11), 6837.

Essien, U. E., Akankpo, A. O., & Igboekwe, M. U. (2014). Poisson's ratio of surface soils and shallow sediments determined from seismic compressional and shear wave velocities. *International Journal of Geosciences*, 5(12), 1540–1546.

GEO-SLOPE International Ltd. (2015). *Seepage modeling with SEEP/W*.

Genevois, R., Tecca, P. R., and Genevois, C. (2022). Mitigation measures of debris flow and landslide risk carried out in two mountain areas of North-Eastern Italy. *Journal of Mountain Science,* 19(6), 1808–1822.

Hazen, A. (1892). Some physical properties of sands and gravels, with special reference to their use in filtration. *24th Annual Report*, Massachusetts State Board of Health, Boston, MA, 539–556.

Lambe, T. W. (1973). "Predictions in soil engineering." *Géotechnique, 23*(2), 151–202.

Obrzud, R. F., and Truty, A. (2018). The Hardening Soil Model: A practical guidebook. *Zace Services, Lausanne,* Switzerland (2018).

Seequent Limited, The Bentley Subsurface Company. (2024). *Stress-strain modeling with GeoStudio*.

Smith, A., Dixon, N., and Fowmes, G. J. (2016). Early detection of first-time slope failures using acoustic emission measurements: Large-scale physical modelling. *Géotechnique*, 66(11), 878–893

van Genuchten, M. (1980). Closed-form equation for predicting the hydraulic conductivity of unsaturated soils. *Soil Science Society of America Journal,* 44(5), 35-53.